Editors' Suggestion | Featured in Physics

Quantized Conductance through a Spin-Selective Atomic Point Contact

Martin Lebrat, Samuel Häusler, Philipp Fabritius, Dominik Husmann, Laura Corman,* and Tilman Esslinger
Department of Physics, ETH Zurich, 8093 Zürich, Switzerland

(Received 7 July 2019; published 8 November 2019)

We implement a microscopic spin filter for cold fermionic atoms in a quantum point contact (QPC) and create fully spin-polarized currents while retaining conductance quantization. Key to our scheme is a near-resonant optical tweezer inducing a large effective Zeeman shift inside the QPC while its local character limits dissipation. We observe a renormalization of this shift due to interactions of only a few atoms in the QPC. Our work represents the analog of an actual spintronic device and paves the way to studying the interplay between spin splitting and interactions far from equilibrium.

DOI: 10.1103/PhysRevLett.123.193605

Coupling the spin of a particle to its motion can unveil its quantum nature, as was demonstrated in the Stern-Gerlach experiment [1]. In condensed-matter systems, this can be achieved via the Zeeman effect or spin-orbit coupling, and it gives rise to a variety of transport phenomena. For instance, magnetic impurities coupled to a metallic or superconducting bath strongly influence resistivity [2,3], and spin-orbit coupling can induce spin-polarized modes and Majorana fermions at the edge of topological materials [4,5].

Cold atoms provide an alternative platform to investigate spin transport with long coherence times and a fine-tuning of interactions by encoding the spin into different hyperfine states. There, spin degeneracy can be lifted with actual magnetic fields or differential Stark shifts [6–8], and spin-orbit coupling can be realized using Raman schemes [9–11]. Experimental realizations have so far addressed spin-dependent effects on a global scale. However, a local manipulation of the spin would allow the study of interfaces, as encountered in magnetic heterojunctions and, in general, represents a central ingredient for spintronics [12], quantum computation [13], and quantum simulation [14].

In this work, we use a quantum gas experiment [15] to probe spin transport through a microscopic one-dimensional channel connected to two macroscopic reservoirs. By focusing a near-resonant optical tweezer inside the channel, we realize an effective Zeeman splitting that is large compared to all other transport energy scales and allows us to individually control spin currents. As the state of the reservoirs is not affected, transport measurements are carried out around a well-defined equilibrium, and we observe spin-polarized quantized conductance. Owing to the local character of the tweezer, we reduce losses caused by photon scattering and increase our experimental timescales to several seconds. This method allows us to detect minute mean-field effects caused by merely two atoms, on average, in the tweezer region. Our results are captured by an extended Landauer-Büttiker model whose validity is studied in a companion paper [16], where regimes with stronger dissipation are explored as well.

We prepare a degenerate cloud of lithium-6 atoms in a balanced mixture of the first- and third-lowest hyperfine states, labeled as pseudospins $|\downarrow\rangle$ and $|\uparrow\rangle$, with about $N = 1.1(1) \times 10^5$ atoms per state at a typical temperature of $T = 66(12)$ nK [17]. A magnetic field is tuned close to $B = 568$ G, where collisional s-wave interactions between $|\downarrow\rangle$ and $|\uparrow\rangle$ vanish. We optically imprint a quantum point contact (QPC) with transverse confinement frequencies of $\nu_x = 14.0(6)$ kHz and $\nu_z = 9.03(5)$ kHz by intersecting two far-detuned repulsive laser beams. The QPC separates the cloud into two reservoirs that act as a source and drain of atoms with typical mean chemical potential $\mu_{\mathrm{res}} = (\mu_L + \mu_R)/2 = k_B \times 0.23\ \mu$K globally fixed by the total atom number. For a noninteracting Fermi gas, the conductance per spin and transverse QPC mode with unit transmission is equal to the conductance quantum $1/h$ [26]. The number of available transport modes is set via a far-detuned attractive gate beam with Gaussian waist $w_g = 31.8(3)\ \mu$m depicted in Fig. 1(a). Its associated potential minimum $-V_g < 0$ is tunable and locally increases the chemical potential μ_{res} to a value $\mu_{\mathrm{res}} - (-V_g) = V_g + \mu_{\mathrm{res}}$.

The control over each individual spin current is achieved using an additional σ^--polarized beam centered on the QPC. Its Gaussian intensity profile is holographically defined by a digital micromirror device and has a waist of $w_s = 2.0(1)\ \mu$m, which is smaller than the QPC length of $5.9(1)\ \mu$m and the typical Fermi wavelength of $\lambda_F = \sqrt{h/m\nu_z} = 2.7\ \mu$m, where m is the mass of a ^{6}Li atom. Its optical frequency ν_s is tuned between the transition frequencies of $|\uparrow\rangle$ and $|\downarrow\rangle$ to the excited manifold $^2P_{3/2}$, inducing a repulsive dipole potential for $|\uparrow\rangle$ and an attractive potential for $|\downarrow\rangle$. For opposite detunings relative to the two transitions, i.e., $\delta_\uparrow = -\delta_\downarrow = 81.3$ MHz, both

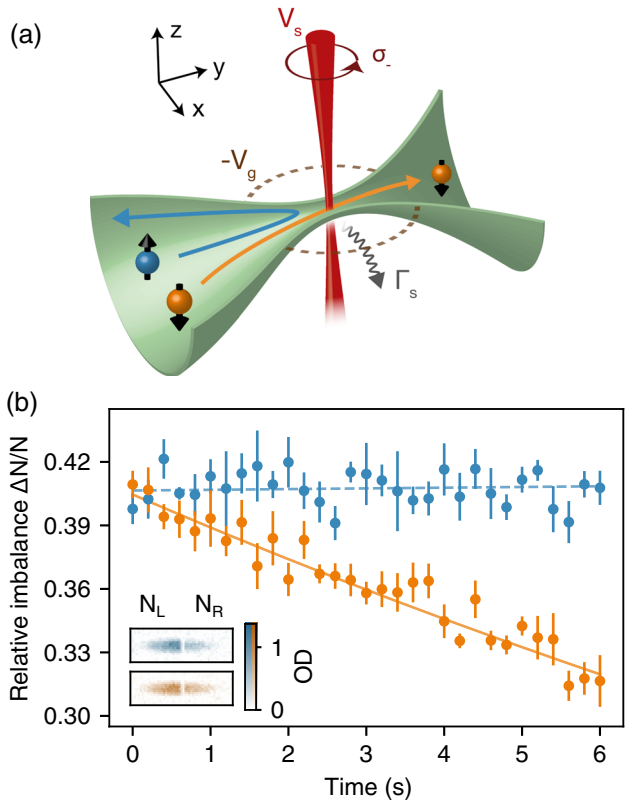

FIG. 1. Creating spin-polarized currents through an atomic QPC. (a) A near-resonant optical tweezer (red) with waist $w_s = 2.0(1)$ μm, which introduces an effective Zeeman shift V_s inside an optically defined QPC (green). This tweezer allows ^{6}Li atoms in the lowest hyperfine state ($|\downarrow\rangle$, orange) to flow between two reservoirs while blocking atoms in the third-lowest state ($|\uparrow\rangle$, blue), thereby acting as a spin filter with losses determined by the photon scattering rate Γ_s. A far-detuned attractive gate beam with negative potential $-V_g$ (dashed circle) locally increases the chemical potential μ_{res} imposed by the reservoirs. (b) Time evolution of the relative atom number difference between the left and right reservoirs $\Delta N/N = (N_L - N_R)/(N_L + N_R)$, obtained for a mean chemical potential $V_g + \mu_{\mathrm{res}} = k_B \times 0.61(2)$ μK and a near-resonant beam power $P_s = 20(6)$ pW, and at a scattering length $a = 0(7)a_0$. It is constant for $|\uparrow\rangle$ and has a decay time of 25(1) s for $|\downarrow\rangle$. The associated currents $I_\uparrow = -19 \pm 85$ atoms/s and $I_\downarrow = 833 \pm 98$ atoms/s indicate fully polarized transport within the fit error. Error bars show the standard error of the mean of five measurements here and in Fig. 2. Inset: Optical density (OD) after 6 s of left and right reservoirs over 970×320 μm, averaged over five absorption images.

dipole potentials have equal magnitudes $\pm V_s$. The magnitudes are linear in the light intensity I_s for $I_s \ll I_{\mathrm{sat}}$, where $I_{\mathrm{sat}} = 25.4$ W/m^2 is the saturation intensity of the transition. The induced light shifts can be viewed as an optical analogue to the Zeeman shift $V_s = -\mu B_z$ of a spin-1/2 particle with magnetic moment μ in a fictitious magnetic field B_z. As opposed to magnetically induced shifts, here atoms scatter photons at a rate Γ_s; this process imparts kinetic energy and leads to losses. The ratio Γ_s/V_s is independent of I_s and equal to 9.4×10^3 s$^{-1}/(k_B\,\mu\mathrm{K})$ for the detuning mentioned above [16].

Starting with equal chemical potential biases across the QPC for both spins, we apply the spin-dependent optical potential to create a spin-polarized current. Typically, we prepare, for each spin state, atom number differences of $\Delta N(0) = 45(3) \times 10^3$ between the two reservoirs and measure their time evolution towards equilibrium. During that time, the s-wave scattering length is set to $a = 0(7)a_0$, where $a_0 = 52.9$ pm is the Bohr radius, and the optical power of the near-resonant tweezer is $P_s = 20(6)$ pW, corresponding to a peak intensity $I_s = 2P_s/\pi w_s^2 = 3(1)$ W/m^2 $= 0.13(4)I_{\mathrm{sat}}$. Over 6 s, the relative atom number difference $\Delta N(t)/N(t)$ remains constant for spin $|\uparrow\rangle$ and is reduced by about one-quarter for spin $|\downarrow\rangle$, with a fitted decay time of $\tau_\downarrow = 25(1)$ s [Fig. 1(b)]. Assuming linear response, we infer currents for each spin of $I_\uparrow = -19 \pm 85$ atoms/s and $I_\downarrow = 833 \pm 98$ atoms/s.

Our scheme thus represents the cold-atom equivalent of a spin filter, a fundamental building block for spintronics previously realized in spin-polarized tunnel junctions [27], quantum point contacts under strong magnetic fields [28], or double-stranded DNA illuminated by polarized light [29]. The current polarization obtained here is comparable within the fitting error to the best values obtained with magnetic heterostructures [30].

Despite a maximal photon scattering rate $\Gamma_s = 3(1) \times 10^3$ s^{-1} at the center of the tweezer, the decrease in total atom number N is limited [Fig. 2(a)]. Losses lead to an overall decrease of the mean chemical potential $\mu_{\mathrm{res}} = (\mu_L + \mu_R)/2$ in the reservoirs by $k_B \times 30$ nK [Fig. 2(b)], much smaller than the other typical energy scales. Meanwhile, no significant increase of temperature T is observed [Fig. 2(c)]. Since the atom-atom mean free path is larger than the system's size, the additional recoil energy $E_R = (h/\lambda)^2/2m = k_B \times 3.54$ μK imparted to atoms scattered by near-resonant photons with wavelength $\lambda = 671$ nm is not deposited in the reservoirs through thermalization. However, as currents and losses are small relative to the global atom number, we expect the reservoirs to remain effectively described by thermal states [16].

Since the macroscopic state of reservoirs is only weakly affected by losses, transport occurs around a well-defined equilibrium, and conductance is related to the single-particle transmission through the QPC according to the Landauer-Büttiker formula [31]. Probing the transmission in a spin- and energy-dependent way allows us, in turn, to estimate the Zeeman shift induced by the near-resonant beam. This estimate can be found by tuning the local chemical potential $V_g + \mu_{\mathrm{res}}$ relative to the potentials experienced by both spins. We perform several conductance measurements at a weak scattering length of $a = 91(7)a_0$ for different values of the gate potential V_g.

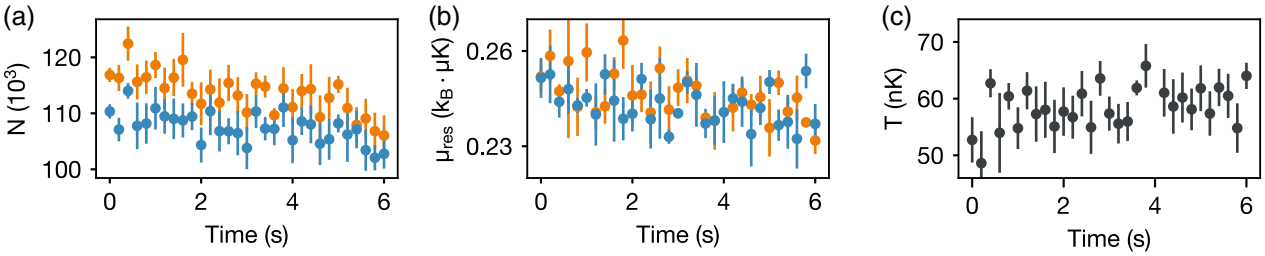

FIG. 2. Evolution of the reservoir thermodynamical quantities. (a) Losses in atom number $N = N_L + N_R$, leading to a small variation of (b) mean reservoir chemical potential $\mu_{\rm res} = (\mu_L + \mu_R)/2$. (c) Mean temperature $T = (T_L + T_R)/2$, which is constant over experimental timescales.

The conductance is inferred from the decay of the relative atom number difference $\Delta N/N$ after a fixed transport time of 4 s [17]. We observe conductance plateaus characteristic of single-mode transport, which overlap when both spins are degenerate [Fig. 3(a)]. Their value of $G = 0.84(1)/h$, slightly below the conductance quantum $1/h$, results from a reduction of the chemical potential bias between the reservoirs due to residual temperature differences, caused by our initial preparation and omitted in the estimation of the conductance.

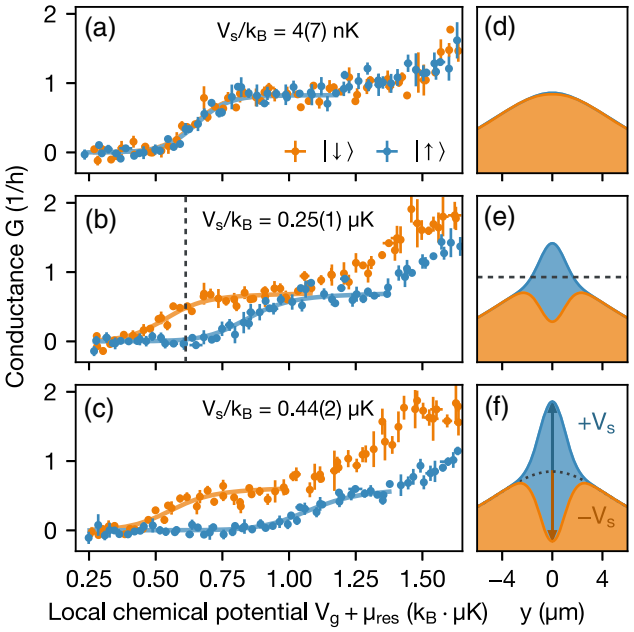

FIG. 3. Lifting the spin degeneracy of the QPC ground state. (a) Conductance G of each spin state at scattering length $a = 91(7)a_0$ versus local chemical potential $V_g + \mu_{\rm res}$ without a near-resonant beam; (b) with peak intensity $I_s = 0.13(4)I_{\rm sat}$ (as in Figs. 1 and 2), where $I_{\rm sat}$ is the D_2-line saturation intensity; (c) with $I_s = 0.17(5)I_{\rm sat}$. Here and in the following, error bars correspond to the standard error of the mean of three measurements. Fits by a Landauer model are shown as solid curves and indicate an increase of the spin-dependent potential up to $V_s = k_B \times 0.44(2)$ μK. (d)–(f) Quasi-1D potentials along the transport direction y. The chemical potential of Figs. 1 and 2 is indicated by dashed lines in (b) and (e).

Upon increasing the near-resonant beam intensity I_s, the conductance plateau for the repelled spin $|\uparrow\rangle$ is shifted towards larger chemical potentials [Figs. 3(b) and 3(c)]. This shift corresponds to the classical barrier $+V_s$ added to the QPC zero-point energy [Fig. 3(d)] by the spin-dependent potential [Figs. 3(e) and 3(f), blue]. An opposite shift is observed for the attracted spin $|\downarrow\rangle$, indicating a weak decrease of the potential barrier due to the near-resonant beam being smaller than the QPC length [Figs. 3(e) and 3(f), orange]. Current polarization is maximal for chemical potentials located between the potential barriers of both spins as in Fig. 1; the value of $V_g + \mu_{\rm res} = k_B \times 0.61(2)$ μK chosen there is shown by a dashed line in Figs. 3(b) and 3(e). We observe that plateaus persist when the intensity I_s is increased to $0.17(5)I_{\rm sat}$, while their value decreases down to $G = 0.55(2)/h$.

We expect transport observables such as conductance to be fundamentally robust against losses since they are only sensitive to scattering at energies close to the Fermi level, which concerns a small fraction of all atoms subject to near-resonant light. In a Landauer picture valid for weak interactions, these losses contribute to decreasing the conductance by the scattering probability. This probability is equal to about 25% at $I_s = 0.13(4)I_{\rm sat}$ for a typical Fermi velocity $v_F = \sqrt{h\nu_z/m} = 2.4$ cm/s in the single-mode regime, and it is compatible with the decrease of the conductance plateau from $G = 0.84(1)/h$ in Fig. 3(a) to $G = 0.72(2)/h$ in Fig. 3(b). In contrast, losses of atoms below the Fermi level do not generate a net current since their average velocity is zero. In the actual setup, these losses represent the majority of the losses shown in Fig. 2(a) (see also Ref. [16]) and only affect transport indirectly through the weak reduction of the chemical potential [Fig. 2(b)].

To extract the spin-dependent potential V_s, we fit the conductances of both states with a Landauer model [solid curves in Figs. 3(a)–3(c)]. The model describes the QPC and spin-dependent gate by two independent quasi-1D potentials shown in Figs. 3(d)–3(f), and it includes a position-dependent photon scattering rate $\Gamma(y)$ as an imaginary part $i\hbar\Gamma(y)/2$ [16]. A linear regression on five different values of I_s yields a conversion ratio $V_s/I_s = 103(17)\mathrm{k_B nK/(W/m^2)}$ compatible with the theoretical

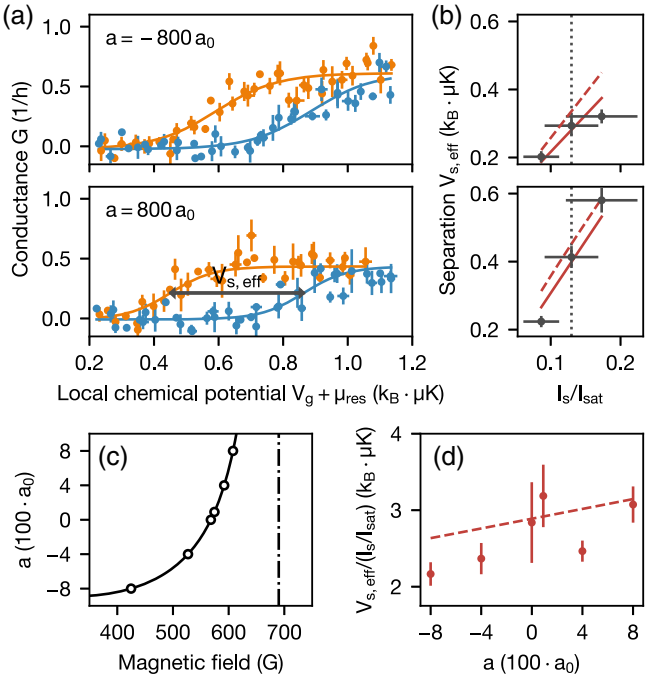

FIG. 4. Effect of 1D interactions on transport. (a) Conductance G at scattering lengths $a = -800.0(7)a_0$ and $a = +800(16)a_0$, near-resonant beam intensity $I_s = 0.13(4)I_{\mathrm{sat}}$, and equal detuning from both states, $\bar{\delta} = 0$. Solid curves indicate fits with a logistic function to extract the energy separation $V_{s,\mathrm{eff}}$. (b) Fitted separation $V_{s,\mathrm{eff}}$ versus I_s normalized by the D_2-line saturation intensity I_{sat}. The vertical dotted line indicates the intensity used in (a). (c) Scattering length a versus magnetic field, tuned to the left of a broad Feshbach resonance (dash-dotted line). The magnetic field is calibrated with a relative uncertainty of 0.1%. (d) Ratio $V_{s,\mathrm{eff}}/(I/I_{\mathrm{sat}})$ versus scattering length a, obtained by linear regression displayed as solid lines in (b). A Hartree mean-field model including a finite temperature of 66 nK is indicated as dashed lines in (b) and (d).

value of $98(3)\mathrm{k_B nK/(W/m^2)}$. We find a maximal potential of $V_s = k_B \times 0.44(2)\ \mu$K, about twice the typical Fermi energy $E_F = h\nu_z/2 = k_B \times 0.22\ \mu$K in the single-mode regime.

Using the broad Feshbach resonance of ^{6}Li, we now investigate how interactions between itinerant atoms passing through the QPC compete with the Zeeman splitting created by the near-resonant tweezer. Interactions renormalize the effective potential felt by each spin, which can be sensitively probed by measuring the energy shifts in the conductance curves. We explore both attractive and repulsive interactions from $a = -800.0(7)a_0$ to $800(16)a_0$ in the nonsuperfluid regime, which are values of the scattering length where interactions are described by mean-field theory (as opposed to previous results obtained in the strongly correlated regime [32]). Figure 4(a) shows conductances for each spin obtained at $a = \pm 800a_0$ and fixed intensity $I_s = 0.13(4)I_{\mathrm{sat}}$ as a function of the local chemical potential $V_g + \mu_{\mathrm{res}}$. We observe a change in the energy separation $V_{s,\mathrm{eff}}$ between the conductance curves by about $k_B \times 0.1\ \mu$K, a shift smaller than the width of the conductance step of $4k_BT = k_B \times 0.26(5)\ \mu$K. The conductance values are reduced compared to Fig. 3(b) as well, which we attribute to slightly increased losses. This visible separation is reduced for attractive interactions and increased for repulsive interactions. We quantify it with a fit by a logistic function motivated by noninteracting Landauer theory for different values of I_s [Fig. 4(b)]. The different slopes $V_{s,\mathrm{eff}}/(I_s/I_{\mathrm{sat}})$, obtained by linear regression, confirm the effect of interactions.

We repeat this measurement for intermediate scattering lengths a [Fig. 4(c)] and extract the ratio $V_{s,\mathrm{eff}}/(I_s/I_{\mathrm{sat}})$ for each interaction strength [Fig. 4(d)]. The data are described by a self-consistent Hartree mean-field model [17], where $|{\downarrow}\rangle$ atoms provide an extra potential proportional to the interaction parameter $U = 2h\sqrt{\nu_x\nu_z}a$ that eases or hinders the passage of $|{\uparrow}\rangle$ atoms depending on its sign. We find good agreement even though the model does not include dissipation and density fluctuations, which may be non-negligible in the 1D region. Crucially, our conductance signal is obtained by probing the QPC with typically a few thousand atoms over 4 s. The mean-field approximation formally relies on replacing operators for atomic densities by their thermodynamical averages, which are about 1 atom per micron and per spin here [17]. Despite the absence of thermodynamical equilibrium in the microscopic QPC, such a thermodynamical average is experimentally mimicked by the effective time average associated with our measurement. Dissipation is likely to play a substantial role for larger interactions [33,34], where both fluctuations and coherence are expected to be stronger within the 1D region [35].

Our work demonstrates how transport measurements are sensitive to minute interaction effects occurring on the scale of the Fermi wavelength from the integration of a weak transport signal. Our capability to spin-engineer potentials can be readily extended to more complex structures [32] and opens avenues for exploring the transport dynamics of strongly correlated systems, where novel nonequilibrium spin and heat transport [36,37] and exotic phases of matter [5] could be observed.

We thank L. Dogra for early theoretical and technical contributions; T. Giamarchi, L. Glazman, H. Moritz, H. Ott, and A.-M. Visuri for helpful discussions; and J.-P. Brantut, R. Citro, M. Landini, J. Mohan, and K. Viebahn for their critical reading of the manuscript. We acknowledge the Swiss National Science Foundation (Projects No. 182650 and No. NCCR-QSIT) and ERC Advanced Grant TransQ (Project No. 742579) for funding. L. C. is supported by the ETH Zurich Postdoctoral Fellowship, the Marie Curie Actions for People COFUND program, and the EU Horizon 2020 Marie Curie TopSpiD (Project No. 746150).

*Corresponding author.
lcorman@phys.ethz.ch

[1] W. Gerlach and O. Stern, Der experimentelle Nachweis der Richtungsquantelung im Magnetfeld, Z. Phys. **9**, 349 (1922).
[2] J. Kondo, Resistance Minimum in Dilute Magnetic Alloys, Prog. Theor. Phys. **32**, 37 (1964).
[3] H. Shiba, Classical Spins in Superconductors, Prog. Theor. Phys. **40**, 435 (1968).
[4] C. L. Kane and E. J. Mele, $\mathbb{Z}_2$ Topological Order and the Quantum Spin Hall Effect, Phys. Rev. Lett. **95**, 146802 (2005).
[5] C. Beenakker, Search for Majorana fermions in superconductors, Annu. Rev. Condens. Matter Phys. **4**, 113 (2013).
[6] P. S. Jessen and I. H. Deutsch, Optical lattices, Adv. At., Mol., Opt. Phys. **37**, 95 (1996).
[7] O. Mandel, M. Greiner, A. Widera, T. Rom, T. W. Hänsch, and I. Bloch, Coherent Transport of Neutral Atoms in Spin-Dependent Optical Lattice Potentials, Phys. Rev. Lett. **91**, 010407 (2003).
[8] A. Steffen, A. Alberti, W. Alt, N. Belmechri, S. Hild, M. Karski, A. Widera, and D. Meschede, Digital atom interferometer with single particle control on a discretized space-time geometry, Proc. Natl. Acad. Sci. U.S.A. **109**, 9770 (2012).
[9] Y.-J. Lin, K. Jiménez-García, and I. B. Spielman, Spin-orbit-coupled Bose-Einstein condensates, Nature (London) **471**, 83 (2011).
[10] P. Wang, Z.-Q. Yu, Z. Fu, J. Miao, L. Huang, S. Chai, H. Zhai, and J. Zhang, Spin-Orbit Coupled Degenerate Fermi Gases, Phys. Rev. Lett. **109**, 095301 (2012).
[11] L. W. Cheuk, A. T. Sommer, Z. Hadzibabic, T. Yefsah, W. S. Bakr, and M. W. Zwierlein, Spin-Injection Spectroscopy of a Spin-Orbit Coupled Fermi Gas, Phys. Rev. Lett. **109**, 095302 (2012).
[12] I. Žutić, J. Fabian, and S. Das Sarma, Spintronics: Fundamentals and applications, Rev. Mod. Phys. **76**, 323 (2004).
[13] D. Loss and D. P. DiVincenzo, Quantum computation with quantum dots, Phys. Rev. A **57**, 120 (1998).
[14] E. Jané, G. Vidal, W. Dür, P. Zoller, and J. I. Cirac, Simulation of quantum dynamics with quantum optical systems, Quantum Inf. Comput. **3**, 15 (2003).
[15] S. Krinner, T. Esslinger, and J.-P. Brantut, Two-terminal transport measurements with cold atoms, J. Phys. Condens. Matter **29**, 343003 (2017).
[16] L. Corman, P. Fabritius, S. Häusler, J. Mohan, L. H. Dogra, D. Husmann, M. Lebrat, and T. Esslinger, companion paper, Quantized conductance through a dissipative atomic point contact, Phys. Rev. A **100**, 053605 (2019).
[17] See Supplemental Material at http://link.aps.org/supplemental/10.1103/PhysRevLett.123.193605 for details, which includes Refs. [18–25].
[18] C. H. Schunck, M. W. Zwierlein, C. A. Stan, S. M. F. Raupach, W. Ketterle, A. Simoni, E. Tiesinga, C. J. Williams, and P. S. Julienne, Feshbach resonances in fermionic ^{6}Li, Phys. Rev. A **71**, 045601 (2005).
[19] S. Häusler, S. Nakajima, M. Lebrat, D. Husmann, S. Krinner, T. Esslinger, and J.-P. Brantut, Scanning Gate Microscope for Cold Atomic Gases, Phys. Rev. Lett. **119**, 030403 (2017).
[20] P. T. Boggs and J. E. Rogers, Orthogonal distance regression, Contemp. Math. **112**, 183 (1990).
[21] S. Krinner, M. Lebrat, D. Husmann, C. Grenier, J.-P. Brantut, and T. Esslinger, Mapping out spin and particle conductances in a quantum point contact, Proc. Natl. Acad. Sci. U.S.A. **113**, 8144 (2016).
[22] G. Su, J. Chen, and L. Chen, Low-temperature behavior of a weakly interacting Fermi gas trapped in a power-law potential, Phys. Lett. A **315**, 109 (2003).
[23] F. W. J. Olver, D. W. Lozier, R. F. Boisvert, and C. W. Clark, *NIST Handbook of Mathematical Functions* (Cambridge University Press, Cambridge, England, 2010).
[24] J. Stephenson, Fluctuations in particle number in a grand canonical ensemble of small systems, Am. J. Phys. **42**, 478 (1974).
[25] K. Mølmer, Y. Castin, and J. Dalibard, Monte-Carlo wave-function method in quantum optics, J. Opt. Soc. Am. B **10**, 524 (1993).
[26] S. Krinner, D. Stadler, D. Husmann, J.-P. Brantut, and T. Esslinger, Observation of quantized conductance in neutral matter, Nature (London) **517**, 64 (2015).
[27] R. Meservey and P. M. Tedrow, Spin-polarized electron tunneling, Phys. Rep. **238**, 173 (1994).
[28] C. Rössler, S. Baer, E. d. Wiljes, P.-L. Ardelt, T. Ihn, K. Ensslin, C. Reichl, and W. Wegscheider, Transport properties of clean quantum point contacts, New J. Phys. **13**, 113006 (2011).
[29] B. Göhler, V. Hamelbeck, T. Z. Markus, M. Kettner, G. F. Hanne, Z. Vager, R. Naaman, and H. Zacharias, Spin selectivity in electron transmission through self-assembled monolayers of double-stranded DNA, Science **331**, 894 (2011).
[30] C. H. Marrows, Spin-polarised currents and magnetic domain walls, Adv. Phys. **54**, 585 (2005).
[31] S. Datta, Electronic Transport in Mesoscopic Systems, *Cambridge Studies in Semiconductor Physics and Microelectronic Engineering* (Cambridge University Press, Cambridge, England, 1995).
[32] M. Lebrat, P. Grišins, D. Husmann, S. Häusler, L. Corman, T. Giamarchi, J.-P. Brantut, and T. Esslinger, Band and Correlated Insulators of Cold Fermions in a Mesoscopic Lattice, Phys. Rev. X **8**, 011053 (2018).
[33] M. Müller, S. Diehl, G. Pupillo, and P. Zoller, in *Advances in Atomic, Molecular, and Optical Physics*, edited by P. Berman, E. Arimondo, and C. Lin (Academic Press, New York, 2012), Vol. 61, pp. 1–80.
[34] A. J. Daley, Quantum trajectories and open many-body quantum systems, Adv. Phys. **63**, 77 (2014).
[35] H. Fröml, A. Chiocchetta, C. Kollath, and S. Diehl, Fluctuation-Induced Quantum Zeno Effect, Phys. Rev. Lett. **122**, 040402 (2019).
[36] G. E. W. Bauer, E. Saitoh, and B. J. v. Wees, Spin caloritronics, Nat. Mater. **11**, 391 (2012).
[37] F. S. Bergeret, M. Silaev, P. Virtanen, and T. T. Heikkilä, Colloquium: Nonequilibrium effects in superconductors with a spin-splitting field, Rev. Mod. Phys. **90**, 041001 (2018).